Journal of Alzheimer's Disease 86 (2022) 1805–1816
DOI 10.3233/JAD-215596
IOS Press

Characterizing Network Selectiveness to the Dynamic Spreading of Neuropathological Events in Alzheimer's Disease

Wenchao Li[a], Defu Yang[a,b,*], Chenggang Yan[a], Minghan Chen[c], Quefeng Li[d], Wentao Zhu[b,*] and Guorong Wu[e,f] for the Alzheimer's Disease Neuroimaging Initiative[1]

[a]*Intelligent Information Processing Laboratory, Hangzhou Dianzi University, Hangzhou, China*
[b]*Research Center for Healthcare Data Science, Zhejiang Lab, Hangzhou, Zhejiang, China*
[c]*Department of Computer Science, Wake Forest University, Winston-Salem, NC, USA*
[d]*Department of Biostatistics, University of North Carolina at Chapel Hill, Chapel Hill, NC, USA*
[e]*Department of Psychiatry, University of North Carolina at Chapel Hill, Chapel Hill, NC, USA*
[f]*Department of Computer Science, University of North Carolina at Chapel Hill, Chapel Hill, NC, USA*

Accepted 28 January 2022
Pre-press 28 February 2022

Abstract.
Background: Mounting evidence shows that the neuropathological burdens manifest preference in affecting brain regions during the dynamic progression of Alzheimer's disease (AD). Since the distinct brain regions are physically wired by white matter fibers, it is reasonable to hypothesize the differential spreading pattern of neuropathological burdens may underlie the wiring topology, which can be characterized using neuroimaging and network science technologies.
Objective: To study the dynamic spreading patterns of neuropathological events in AD.
Methods: We first examine whether hub nodes with high connectivity in the brain network (assemble of white matter wirings) are susceptible to a higher level of pathological burdens than other regions that are less involved in the process of information exchange in the network. Moreover, we propose a novel linear mixed-effect model to characterize the multi-factorial spreading process of neuropathological burdens from hub nodes to non-hub nodes, where age, sex, and *APOE4* indicators are considered as confounders. We apply our statistical model to the longitudinal neuroimaging data of amyloid-PET and tau-PET, respectively.
Results: Our meta-data analysis results show that 1) AD differentially affects hub nodes with a significantly higher level of pathology, and 2) the longitudinal increase of neuropathological burdens on non-hub nodes is strongly correlated with the connectome distance to hub nodes rather than the spatial proximity.
Conclusion: The spreading pathway of AD neuropathological burdens might start from hub regions and propagate through the white matter fibers in a prion-like manner.

Keywords: Alzheimer's disease, brain networks, hub node, linear mixed-effect model, longitudinal neuroimages

[1]Data used in preparation of this article were obtained from the Alzheimer's Disease Neuroimaging Initiative (ADNI) database (http://adni.loni.usc.edu). As such, the investigators within the ADNI contributed to the design and implementation of ADNI and/or provided data but did not participate in analysis or writing of this report. A complete listing of ADNI investigators can be found at: http://adni.loni.usc.edu/wp-content/uploads/how_to_apply/ADNI_Acknowledgement_List.pdf.

*Correspondence to: Defu Yang, Intelligent Information Processing Laboratory, Hangzhou Dianzi University, Hangzhou 310018, China. E-mail: dfyang@hdu.edu.cn and Wentao Zhu, Research Center for Healthcare Data Science, Zhejiang Lab, Hangzhou, 311122, China. E-mail: zhuwentao.ee@gmail.com.

INTRODUCTION

Alzheimer's disease (AD) is a common neurodegenerative disease with long progression and multi-domain symptoms [1]. Since the brain alterations start much earlier than the onset of clinical symptoms, the availability of reliable biomarkers is critical to achieving an early diagnosis of AD in the preclinical stage. In the AD research framework, major biomarkers include amyloid plaque, neurofibrillary tangle, and neurodegeneration [2–4]. With the rapid development of neuroimaging techniques, we can quantify AD biomarker levels *in vivo* for the whole brain using positron emission tomography (PET) imaging. Considerable efforts on the spatial pattern of imaging biomarkers have contributed to understanding the pathophysiological mechanism of AD. However, the focus of research interest has shifted to study the spreading pathways of neuropathological burdens throughout the brain.

The human brain is a complex system where multiple brain regions are inter-connected and thus form a self-organized brain network. In the view of brain anatomy, the distinct brain regions are physically wired by white matter fibers. Multiple lines of AD investigations have demonstrated the evidence of selective vulnerability from the micro-scale nervous system to the macro-scale brain network [5–9]. For instance, subpopulations of neurons in different brain areas have been found susceptible to specific environmental or pathological injuries that may lead to cell dysfunction or neuron death [8]. Several longitudinal studies further confirm that the disease progression follows vulnerable fiber pathways rather than spatial proximity [10–12]. Since the human brain can be divided into different regions according to cellular systems that contain functionally similar neurons, neural activities can be characterized in a network representation that consists of nodes (brain regions) and edges (their interactions). Hence, selective vulnerability has also been reported in many network analysis studies [13–19]. Specifically, the brain network is a complex system, and several recent studies show that multiple neuropathological factors residing on the system are also interacted and progressed following the connectome pathways [20–23].

In this work, we focus on the selectivity of spreading pathways, with particular attention to the role of network structure in distributing the neuropathological burdens. In the network neuroscience area, there is a wide consensus that the human brain network bears the small-world property [24]. In this regard, it is common to find a small set of hub nodes that have a much higher degree of connectivity than other nodes, indicating a hierarchical system of information processing. Considering the significance of hub nodes in information exchange, it is worthwhile to examine whether hub nodes accumulate a higher level of pathology than non-hub nodes. Validating this hypothesis will allow us to further characterize the propagation of neuropathological events from hub to non-hub nodes and unravel the multivariate factors behind the spreading patterns. To do so, we propose a linear mixed-effect model to investigate whether the propagation of neuropathological burdens follows the connectome path in the brain network.

We will apply the above statistical analysis to the large-scale longitudinal neuroimaging dataset from the Alzheimer's Disease Neuroimaging Initiative (ADNI) database. Following the biomarker framework of AD, we examine the hypotheses of network selectivity and network-based propagation using amyloid-PET (A-biomarker), tau-PET (T-biomarker), and FDG-PET (N-biomarker), where each modality has multiple follow-up scans from an individual subject. Our analysis shows that A-T-N biomarkers manifest selective patterns, although the spatial distributions vary across biomarkers (modalities). Furthermore, we find converging evidence that the distribution of neuropathological burdens is highly related to the connectome path for all biomarkers, which is aligned with the current neuroscience findings that pathological proteins spread in a prion-like manner.

MATERIALS AND METHODS

Participants

Here, after image quality control, 1,439 subjects with longitudinal neuroimaging data are selected from the ADNI dataset, where includes the following multiple scans: T1-weighted MRI, DWI, amyloid-PET, tau-PET, and FDG-PET. Based on the diagnosis label, we partition the whole population into the following groups of normal control (NC), mild cognitive impairment (MCI), and AD. Note that not all participants have complete data for all the five modalities, where the detailed demographic information is listed in Table 1.

Data processing

For each subject, the multi-modal PET images are aligned to the space of T1-weighted MR image at

Table 1
Demographic information

		NC	MCI	AD	Total
Amyloid-PET	Scan number	434	329	430	1,193
	Age (y)	73.1 ± 6.1	71.6 ± 7.4	73.4 ± 7.8	72.8 ± 7.1
	Gender (M/F)	196/238	184/145	250/180	630/563
	Education (y)	16.7 ± 2.6	16.1 ± 2.7	16.0 ± 2.7	16.3 ± 2.7
Tau-PET	Scan number	302	113	110	525
	Age (y)	71.3 ± 5.9	70.7 ± 7.2	72.0 ± 7.9	71.3 ± 6.7
	Gender (M/F)	124/178	69/44	62/48	255/270
	Education (y)	16.9 ± 2.3	16.3 ± 2.8	15.7 ± 2.6	16.5 ± 2.5
FDG-PET	Scan number	446	331	662	1,439
	Age (y)	73.8 ± 5.9	71.4 ± 7.4	74.0 ± 7.7	73.3 ± 7.2
	Gender (M/F)	215/231	183/148	396/266	794/645
	Education (y)	16.4 ± 2.7	16.0 ± 2.7	15.8 ± 2.9	16.0 ± 2.8

the baseline. After the spatial alignment, we applied the following processing steps to obtain the region parcellations from the MR image using FreeSurfer [25]: 1) skull stripping; 2) tissue segmentation; 3) constructing of cortical surface based on the segmentation results; 4) parcellation of the cortical surface, where parcellation of the cortical surface into 148 brain regions based on the Destrieux atlas [26]. According to parcellation results, we applied surface seed based probabilistic fiber tractography between pairwise brain regions, and then produced a 148×148 anatomical connectivity matrix [26]. Brain networks commonly consist of many peripheral regions and a few central ones, i.e., hubs, that play a critical role in organizing and exchanging hierarchical information. At each node, we calculate the network nodal measurements, such as within-module degree z-score, page-rank, and betweenness centrality, to characterize the network topologies using MATLAB-based brain connectivity toolbox (https://sites.google.com/site/bctnet/). In this work, we apply the composite score of betweenness and nodal degree [27] to select hub nodes, where these two metrics are equal to contribute to the composite score. Specifically, we first calculate the centralities of betweenness and nodal degree for each node. Then, normalize these two metrics to the range of 0 to 1. Lastly, ten nodes with the highest composite score are designated as hub nodes. In Fig. 1, we show the screening metrics (betweenness (left) and degree (right)) used to select hub nodes.

After the amyloid-PET, tau-PET, and FDG-PET images are aligned with the corresponding MRI images, it is a common practice to calculate their SUVR (standard uptake value ratio) for each brain region by using the following steps: 1) parcellate the PET image into 148 regions according to the region parcellation results of MRI; 2) calculate the SUV for each brain region by applying a bootstrapping strategy, where we randomly sample a number of voxels from each brain region and then select the top-ranked voxels as the candidates to calculate their mean SUV; 3) repeat step (2) 10000 times and average them as the final SUV level for each brain region; 4) calculate the SUV for the cerebellum region by applying the bootstrapping method used in steps (2) and (3); 5) calculate the SUVR for each brain region by using the ratio of SUV at each brain region between the SUV at cerebellum region. Figure 2 shows the population-average spatial mapping of whole-brain SUVR for amyloid-, tau-, and FDG-PET (from top to bottom) in NC, MCI, and AD groups (from left to right).

Statistical analysis

To fully test the hypothesis that hub nodes are prone to accumulate a higher level of pathology than the non-hub nodes in the brain network, two different methods are used to exploit different data latent information. One is the linear regression method, while the other is the distribution induction method of large sample data.

In the field of AD pathology research, Amyloid-PET (A), Tau-PET (T), and FDG-PET (N) belong to the ATN framework proposed by the 2018 National Institute on Aging-Alzheimer's Association (NIA-AA) [2]. They are three kinds of typical biomarkers widely recognized and applied [28]. Graph-theoretic measures are widely used in the analysis of brain network characteristics, such as the recognition of hub nodes of the brain network. The above knowledge is then used as a framework to separately combine the three centrality measures at each node in the brain network and the distribution characteristics of the three kinds of biomarkers in the corresponding brain region to test the rationality of the above-mentioned

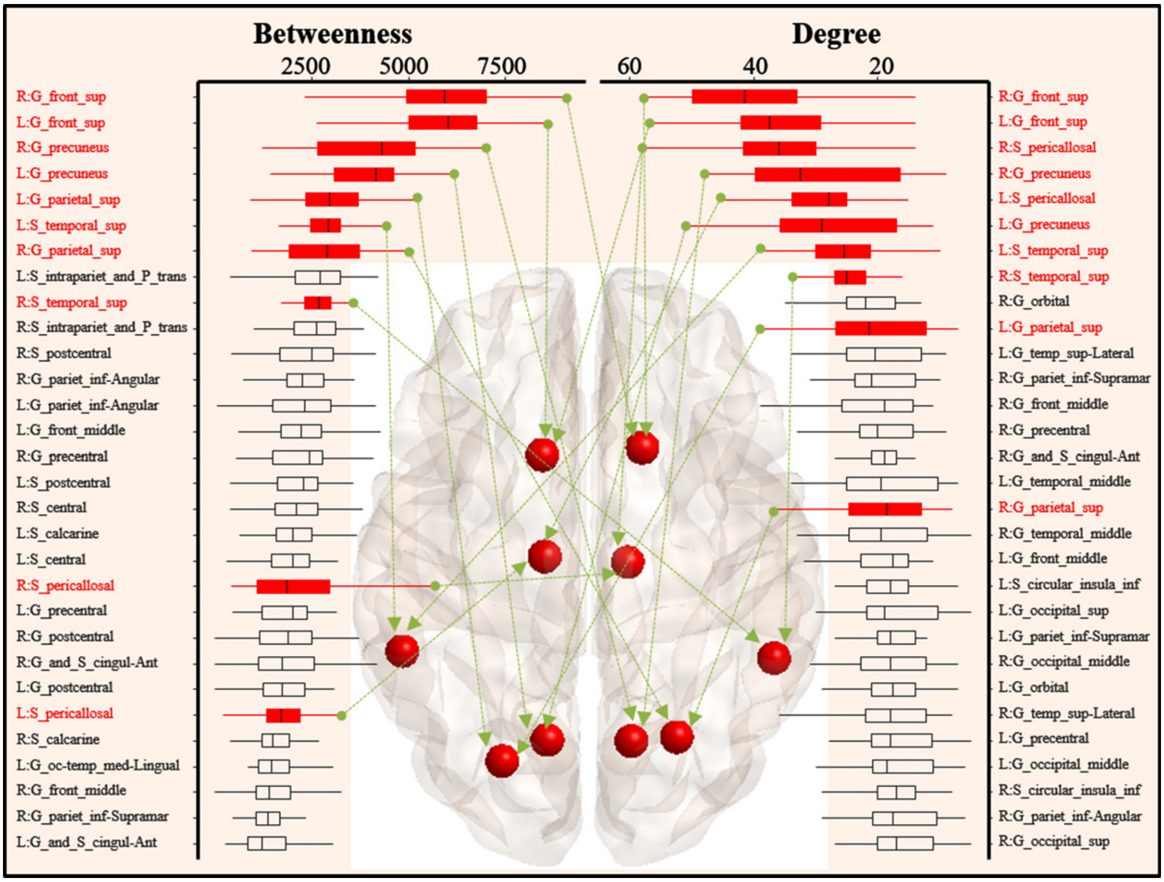

Fig. 1. Population distribution graph of betweenness and degree centrality at each node. The top 30 of 148 nodes are displayed in order from high to low according to the centrality measure. 'R' and 'L' in front of the nodal name indicate the left and right hemispheres, respectively. The selected hub nodes are highlighted in red, which include G_front_sup (Superior frontal gyrus), G_parietal_sup (Superior parietal lobule), G_precuneus (Precuneus gyrus), S_pericallosal (Pericallosal sulcus), and S_temporal_sup (Superior temporal sulcus).

hypothesis. As shown in Fig. 3, the first method regresses the neurodegeneration level at each node (measured by the SUVR level of the above three kinds of AD biomarkers) along with the corresponding network metrics such as within-module degree z-score, PageRank, and nodal betweenness centrality [27]. Specifically, within-module degree z-score and PageRank both reflect the local topological property of the brain network, while nodal betweenness reflects the global topological property of the brain network. Different graph-theoretic metrics of brain networks help reflect different underlying mechanisms of pathological propagation.

In the second method, to more directly access the contrasting aggressiveness of AD towards different brain regions, brain nodes are first divided into two groups: hub nodes or non-hub nodes [29], in which hub nodes are generally highly connected [30] and are associated with brain regions that have important roles in cognitive and executive functions. The hub nodes of brain networks are identified by applying a commonly used consensus classification method, which incorporates several graph-theoretic metrics [29]. To reveal the progressive effect of AD pathology on brain network topology properties, subjects are divided into NC, MCI cohort, and AD cohorts according to individual's disease status, as shown in Table 1. The SUVR levels of three AD biomarkers (amyloid-β, tau, or FDG) are then computed for hub and non-hub nodes, as well as the corresponding standard deviations in each cohort. Figure 4 illustrates the scatter characteristics of SUVR levels at hub and non-hub nodes for each cohort. A *t*-test is performed to demonstrate the significance of cohort differences.

Although a large amount of data are collected and studied in this work, it remains a very small proportion in comparison to the total AD population. To verify the rationality of the above results and to

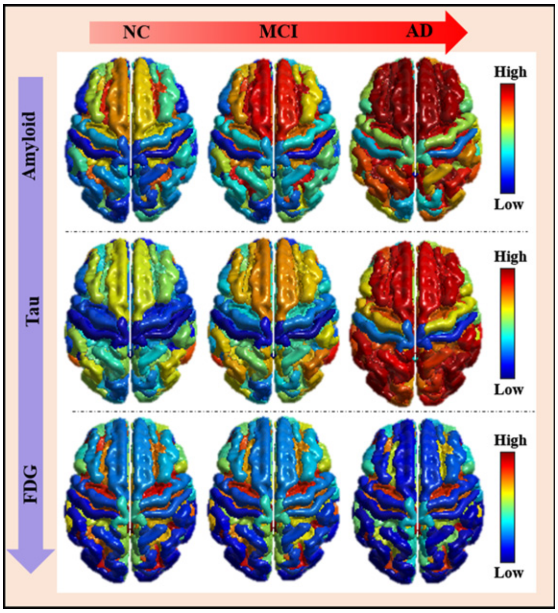

Fig. 2. Regional SUVR level of amyloid, tau, and FDG. On the first two rows of the image, as the disease becomes more severe (NC→MCI→AD), the mean level of amyloid and tau in the corresponding brain areas shows an overall upward trend. The result for FDG in the last row is exactly opposite that of the first two biomarkers, which is in line with existing research.

eliminate as much random interference as possible, the bootstrap method is utilized to generate samples for each cohort. Figure 5 plots the density graph of average SUVR levels using bootstrap samples at hub and non-hub nodes.

Linear mixed-effect model

To test the hypothesis that the propagation of neuropathological burdens follows the connectome path in the brain network, we propose the following linear mixed-effect model to examine whether the differences of neurodegeneration burden between hub nodes and non-hub nodes are strongly related to their topological distance or their spatial distance.

First, define the model variables and parameters. Assume that the brain network contains a total of N nodes, of which H are hub nodes (represented as $V = \{v_h \,|h = 1, \ldots, H\}$), and the remaining M are non-hub nodes (represented as $U = \{u_m \,|m = 1, \ldots, M\}$). The neurodegeneration in AD can be characterized by the accumulation of pathological proteins across various brain regions. Investigating the potential relationship between SUVR levels of pathological proteins at non-hub nodes and hub nodes, we are able to characterize the propagation mechanism of AD. Specifically, the difference between SUVR on hub node v_h measured at the baseline and the counterpart non-hub node u_m at the j^{th} follow-up scan is denoted by $\Delta s^i_{j,m\to h}$. We use d^i_{mh} to characterize the distance between hub node v_h and non-hub node u_m. Specifically, we calculate network topological distance (e.g., the shortest distance in the graph) and spatial distance (e.g., Euclidean distance between the centers of two underlying brain regions) respectively, to test the hypothesis whether the spreading of pathological burden follows the connectome pathway in a prion-like manner or diffuse along with the spatial neighborhood. Since it is reasonable to assume that the brain structure does not change significantly in the disease progression, we only model the distance term d^i_{mh} at the baseline for each subject i and assume d^i_{mh} is fixed in our longitudinal model. Considering the effect of demographic and genetic factors on AD progression, we include in the model the subject-specific *APOE4* biomarker x_{ApoE4} (1: carrier and 0: non-carrier), age x_{Age} (in years), education level x_{Edu} (in years), and gender x_{Gen} (1: male and 0: female). Since subjects in this study constitute a subset randomly sampled from a large-scale AD population, we add the individual random effect of the i^{th} subject, denoted by b^i. Thus, the linear mixed-effect model is constructed as follows:

$$\Delta s^i_{j,m\to h} = \beta_0 + \beta_1 d^i_{mh} + \beta_2 x^i_{ApoE4} + \beta_3 x^i_{Age} + \beta_4 x^i_{Edu} + \beta_5 x^i_{Gen} + \beta_6 \Delta t^i_j + b^i + \varepsilon^i_j, \quad (1)$$

where Δt^i_j is the time gap between the j^{th} follow-up scan and the baseline in i^{th} subject. Our mix-effect model in Eq. (1) assumes that the individual random effect follows a Gaussian distribution, i.e., $b^i \sim N\left(\mu^i, \delta\sigma^2_i\right)$. The restricted maximum-likelihood (REML) estimation is used to estimate the fixed-effects parameters $\{\beta_1, \ldots, \beta_6\}$, and their significance is assessed using the t-test. Furthermore, we use the False Discovery Rate (FDR) approach to create the adjusted p-values (i.e., q-values).

We apply our mixed-effect model to A, T, and N biomarkers separately. In each model, we model the network topology distance and spatial distance one by one. After comprehensively analyzing the obtained model parameters along with the corresponding p-values, the above-mentioned hypothesis can be tested, providing insight into the pathological propagation pattern of AD-related neurodegeneration. When applying the model to different hub nodes separately, if significant β_1 (differs from 0) occurs

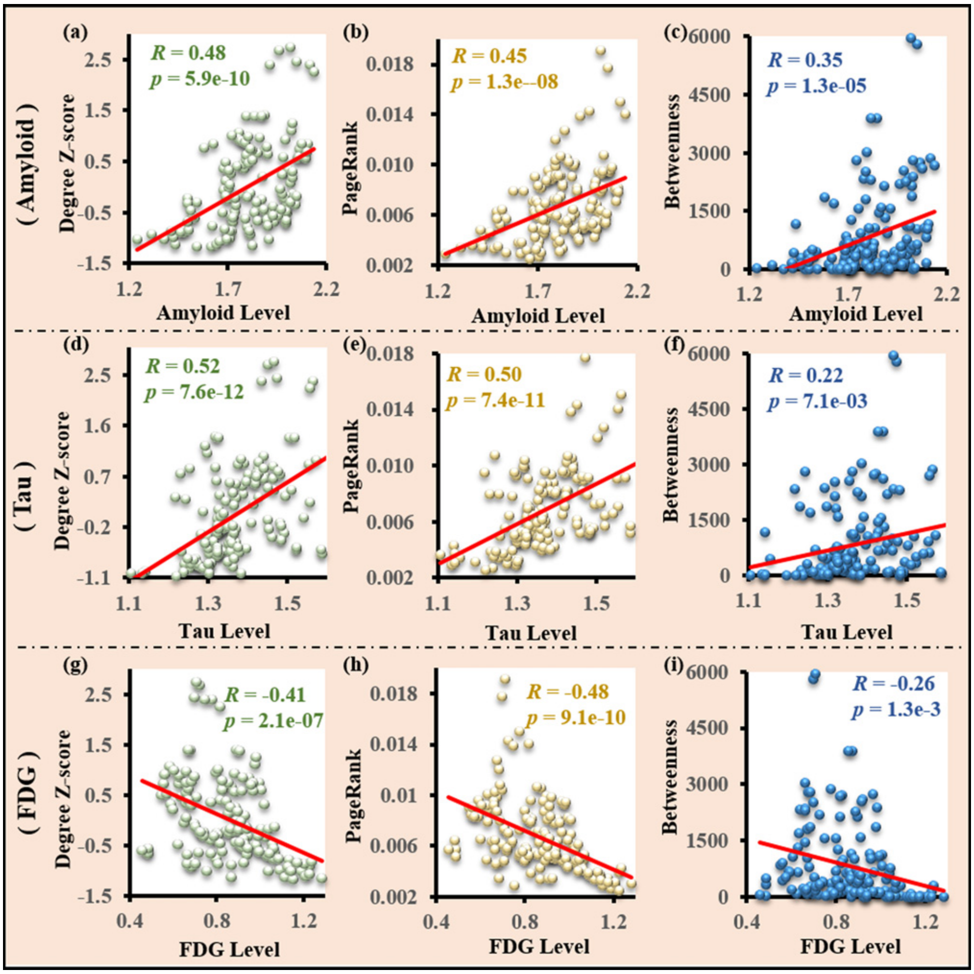

Fig. 3. Graph-theoretic metrics versus pathological damage (amyloid-β, tau, or FDG) SUVR level at each node of brain network. In each row, the three subfigures in left-to-right order describe the results of the three centrality measures, Degree Z-score, PageRank, and Betweenness. Across the first two rows of the graph, the greater the centrality measure of nodes (i.e., the stronger the hub attribute of nodes), and the higher the amyloid or tau level at the corresponding nodes will tend to be. FDG appears opposite to the first two biomarkers in the last row.

more frequently in network topological distance than spatial distance, we can infer that AD pathology is more likely to propagate from hub to non-hub nodes in a trans-neuron manner, mainly through the connectome pathway rather than spatially adjacent tissue.

RESULTS

Network vulnerability under the collection of A-T-N biomarkers

The central hypothesis of our work is to examine whether the AD-related pathological events affect the hub nodes and non-hub nodes differentially in the brain. Since the hub nodes are located at the critical area of the brain network, these nodes can be distinguished via the higher degree of topological measurements such as within-module degree z-score, PageRank, and betweenness [27]. In this context, we first evaluate the correlation between such network measurements and the A-T-N biomarker levels. As shown in Fig. 3, we display the linear correlation result between each biomarker (row-wise) and network measurement (column-wise). It is apparent that 1) the correlation is strong as indicated by the small *p*-values and robust as indicated by the large R-squared value, 2) the correlation is aligned with the current neuroscience findings of the pathophysiological mechanism of AD. Specifically, higher pathological burdens (such as amyloid plaques and neurofibrillary tangles) have higher chance to accumulate the nodes with denser connectivity degrees.

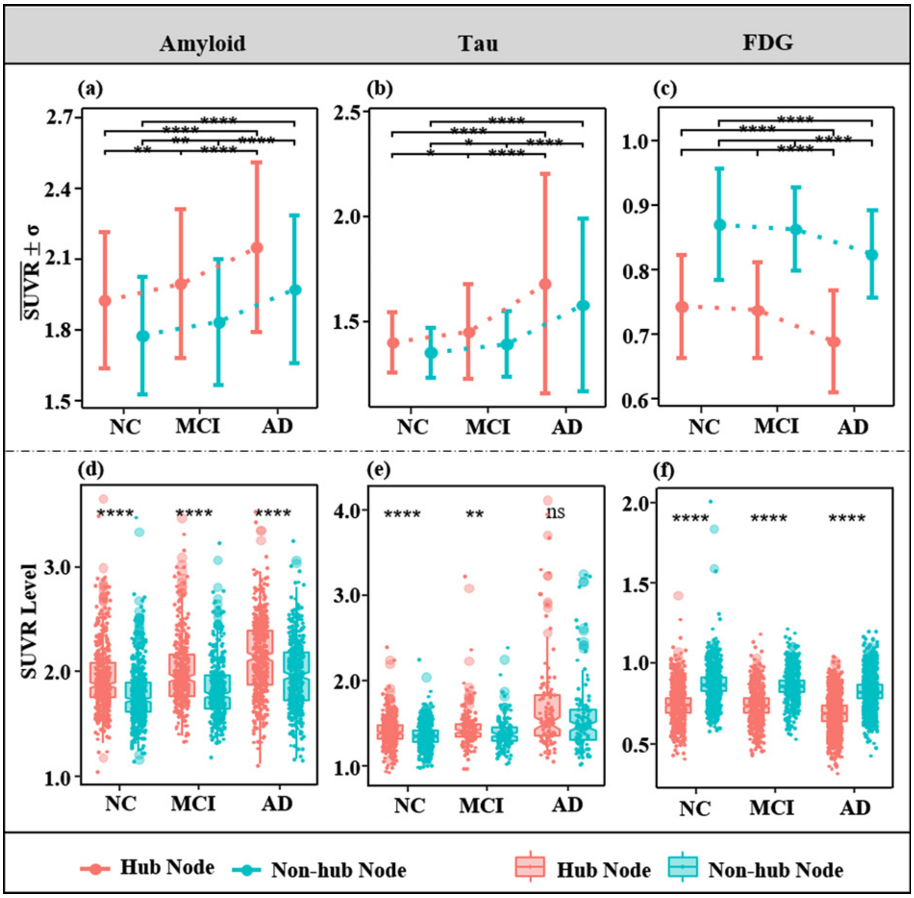

Fig. 4. Distribution of pathological damage in different cohorts. In subfigures a, b, and c, all the bold dots separately depict the average SUVR level of AD biomarkers (amyloid-β, tau, or FDG) at hub (red) and non-hub (green) nodes of brain networks from all subjects in each cohort, with the corresponding bars representing their standard deviation. In subfigures d, e, and f, the box plots show the average distributions of AD biomarker SUVR level at hub nodes (in red) and non-hub nodes (in green) in each cohort.

As a result, greater neurodegeneration (reflected by the lower metabolism level) occurs at the nodes with a higher degree of within-module degree z-score, PageRank, and betweenness (shown in the last row of Fig. 3).

As pathological proteins spread in a trans-neuron way, hub nodes (i.e., brain areas with more adjacent nodes and through which more shortest paths circulate) are more likely to receive toxic proteins from other nodes in the same brain network during the pathological propagation. Following this clue, we carry out the paired *t*-test between hub nodes and non-hub nodes for each A-T-N biomarker. Specifically, we first stratify the aging population into NC, MCI, and AD groups. For each clinic group, we examine whether the amyloid or tau pathology is at a significantly higher level than the non-hub nodes. As shown in Fig. 4, we find that 1) hub nodes (in red) consistently collect a significantly higher amount of A-T-N biomarker levels than non-hub nodes (in green) at all stages of AD (indicated by the '*' at the bottom of Fig. 4), 2) the increase of amyloid and tau pathologies along the progression of AD is significant ('*' at the top of Fig. 4), and 3) similarly the decrease of metabolism level (measured by FDG-PET) is also significant from NC to MCI and AD.

Moreover, we show the distribution of A-T-N biomarkers (with average and medium value) on the hub and non-hub nodes at the bottom of Fig. 4. Interestingly, the difference of tau burden between the hub and non-hub nodes is significant in NC and MCI stages. However, such difference becomes vanished as the disease progresses to AD, which implies that the tau pathology might start from the hub nodes and then spread all over the brain, leaving no significant

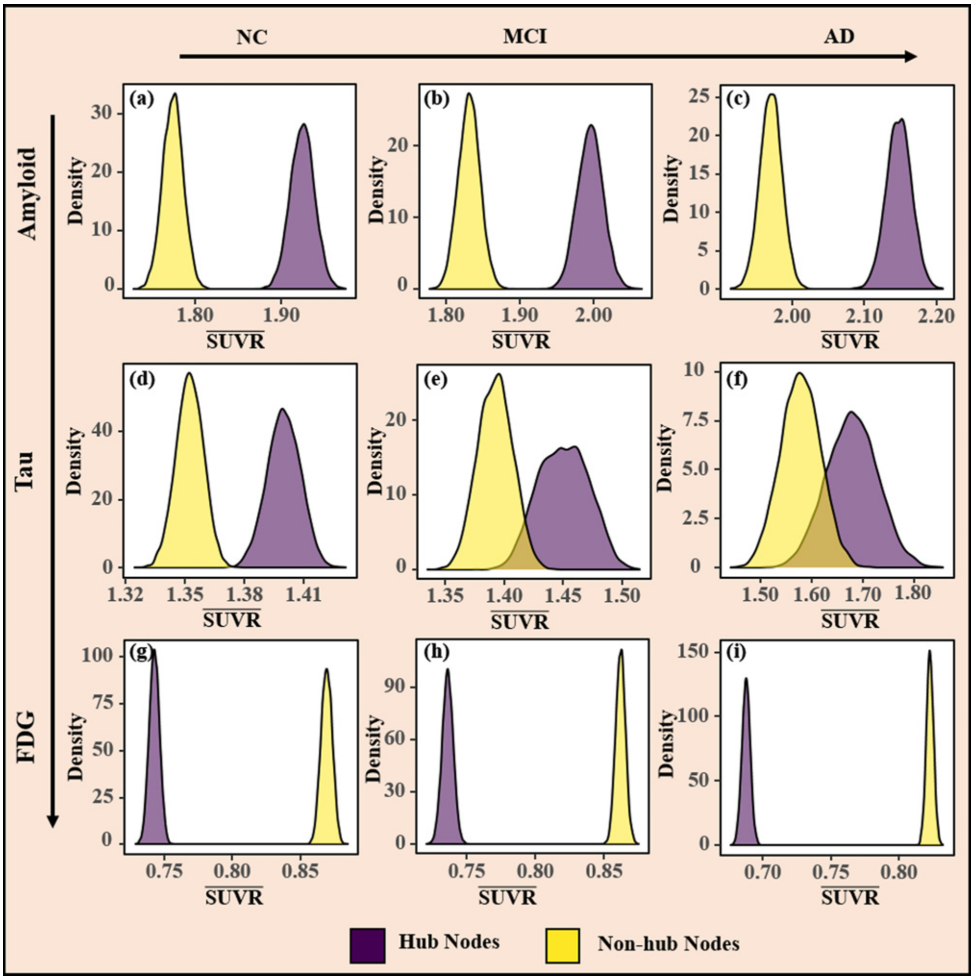

Fig. 5. Density plots of pathological damage levels using bootstrap samples taken from NC, MCI, and AD cohorts. Based on bootstrap samples, subfigures show posterior densities of mean amyloid-β SUVR levels (a,b,c), tau (d,e,f), and FDG (g,h,i). Purple and yellow colors are used to describe the results of the hub and non-hub nodes, respectively.

differences between hub nodes and non-hub nodes at the late stage of AD.

Bootstrap analysis of network vulnerability in AD

To make our analysis more robust, we apply the bootstrap analysis using the resampling strategy. As the density plot shown in Fig. 5, there is no overlap in the estimated densities for the mean value of amyloid-β and FDG SUVR levels between hub node and non-hub node groups for all three cohorts, indicating significant differences between the hub and non-hub node groups for amyloid-β and FDG. Regarding the average tau SUVR level, there is a small amount of overlap in the estimated densities of the hub and non-hub nodes for MCI and AD cohorts, whereas there is almost no overlap in NC cohort. These findings suggest that the difference in the amount of tau neurofibrillary tangles between hub node and non-hub node groups gradually diminishes when transiting from NC to AD stage. In summary, the bootstrap results shown in Fig. 5 are in full agreement with the findings shown in Fig. 4, which provides strong support for the network vulnerability hypothesis that hub nodes are prone to be affected by neuropathological burdens than non-hub nodes.

The prion-like propagation pattern of AD pathological proteins

We select 10 hub nodes (left and right symmetric) out of in total 148 nodes. Figure 6 illustrates the correlation between longitudinal changes of AD

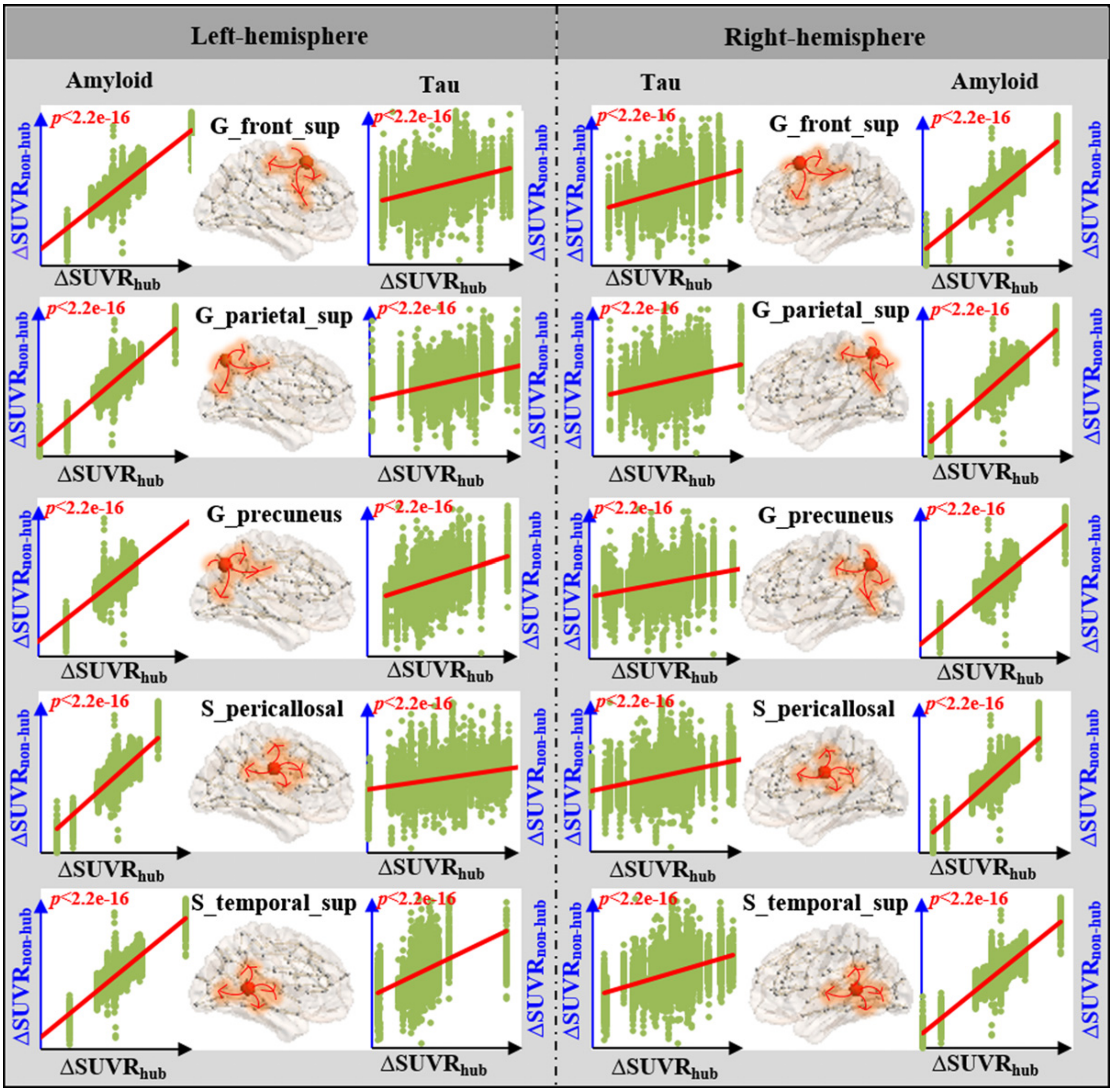

Fig. 6. SUVR level changes of pathological proteins (amyloid-β or tau) at non-hub nodes ($\Delta SUVR_{non\text{-}hub}$) versus SUVR level changes of pathological proteins at the hub node ($\Delta SUVR_{hub}$). The left half of the figure shows the relative results of the five hub nodes in the left hemisphere, and the right half of the figure shows the relative results of the corresponding five hub nodes in the right hemisphere.

pathological proteins at the hub nodes and at non-hub nodes, where the slopes of the linear regression lines are greater than zero. The development of pathological proteins at non-hub nodes is positively correlated with development at the hub node. Intuitively, the results in Fig. 6 implies that the accumulation of pathological burden at the non-hub nodes is largely correlated to the hub nodes to the extent that the pathological proteins at non-hub nodes increase along with the accumulation of pathological proteins at hub nodes in the disease progression.

The propagation mechanism of AD-related neuropathology

Since we find a strong correlation between the occurrence of pathology burdens between the hub and non-hub nodes, we go one step further to investigate the propagation mechanism throughout the brain networks. Specifically, we examine whether the network distance or spatial distance term shows a significant effect in our mixed-effect model in Eq. (1), which uses hub-to-non-hub distance to fit the longitudinal

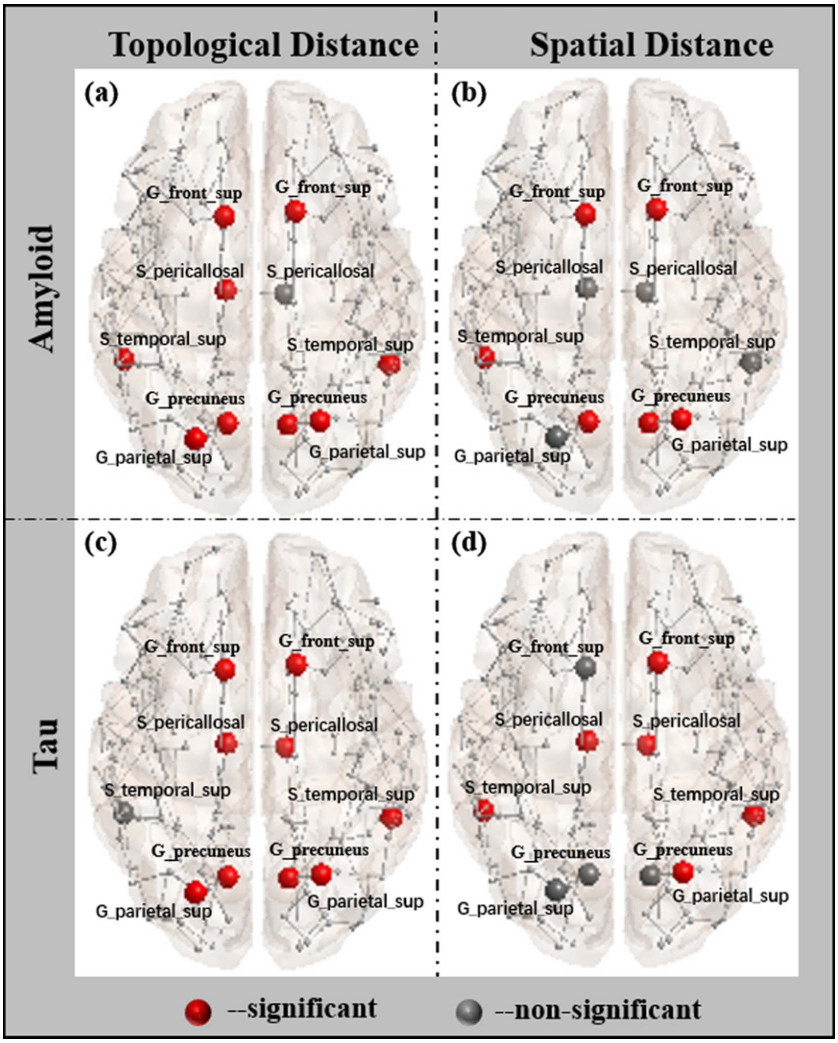

Fig. 7. Hub nodes in the brain. Red nodes indicate that the corresponding regression coefficients β_1 in model (1) are significant to the data associated with the hub node, while grey nodes indicate insignificant model coefficients. The first and second rows depict the results on amyloid and tau, respectively. The left two subfigures (a) and (c) describe the results of the network topological distance, while the right two subfigures describe the results of spatial distance.

change of A-T-N biomarkers. We find that it is more likely that the spreading of amyloid and tau network distance from the hub node to the non-hub nodes follows the wiring patterns of the brain network than the spatial vicinity as much more hub nodes manifest the propagation pattern of spreading to the connected non-hub nodes via the connectome pathways (marked as red dots in Fig. 7a, c) more frequently than using spatial Euclidean distance (Fig. 7b, d).

The results in Fig. 7 are not consistent for amyloid and tau data, partially due to the amyloid and tau might have different pathophysiological mechanisms as reported in a number of existing studies [31, 32]. However, our mixed-effect model shows another piece of evidence that the spreading of neuropathological burdens is in a prion-like manner, that is, one brain region passes on the neuropathologies to the connected brain regions where the intense of propagation depends on the connectivity strength.

DISCUSSION

In this paper, we apply a longitudinal statistical analysis on the large-scale pathology neuroimages. Our findings include 1) AD has a natural "preference" for hub nodes in the brain network; 2) the pathological proteins of AD exhibit a prion-like transmission pattern; 3) AD is more likely to spread through network topological connections as opposed to spatially adjacent connections. As a pilot study, we further examine the role of the non-modifiable genetic determinants (such as *APOE4*) and modifiable lifestyle factors (such as education) in the propagation of A-T-N biomarkers. In our model, education, gender, *APOE4* status, and age are not found significantly associated with the propagation of pathology burdens (both amyloid and tau). Our future work includes applying the model to meta-data analysis with larger sample size.

ACKNOWLEDGMENTS

Data collection and sharing for this project was funded by the Alzheimer's Disease Neuroimaging Initiative (ADNI) (National Institutes of Health Grant U01 AG024904) and DOD ADNI (Department of Defense award number W81XWH-12-2-0012). ADNI is funded by the National Institute on Aging, the National Institute of Biomedical Imaging and Bioengineering, and through generous contributions from the following: AbbVie, Alzheimer's Association; Alzheimer's Drug Discovery Foundation; Araclon Biotech; BioClinica, Inc.; Biogen; Bristol-Myers Squibb Company; CereSpir, Inc.; Cogstate; Eisai Inc.; Elan Pharmaceuticals, Inc.; Eli Lilly and Company; EuroImmun; F. Hoffmann-La Roche Ltd and its affiliated company Genentech, Inc.; Fujirebio; GE Healthcare; IXICO Ltd.; Janssen Alzheimer Immunotherapy Research & Development, LLC.; Johnson & Johnson Pharmaceutical Research & Development LLC.; Lumosity; Lundbeck; Merck & Co., Inc.; Meso Scale Diagnostics, LLC.; NeuroRx Research; Neurotrack Technologies; Novartis Pharmaceuticals Corporation; Pfizer Inc.; Piramal Imaging; Servier; Takeda Pharmaceutical Company; and Transition Therapeutics. The Canadian Institutes of Health Research is providing funds to support ADNI clinical sites in Canada. Private sector contributions are facilitated by the Foundation for the National Institutes of Health (http://www.fnih.org). The grantee organization is the Northern California Institute for Research and Education, and the study is coordinated by the Alzheimer's Therapeutic Research Institute at the University of Southern California. ADNI data are disseminated by the Laboratory for Neuro Imaging at the University of Southern California.

Authors' disclosures available online (https://www.j-alz.com/manuscript-disclosures/21-5596r1).

REFERENCES

[1] Alzheimer's Association (2019) 2019 Alzheimer's disease facts and figures. *Alzheimers Dement* **15**, 321-387.

[2] Jack CR, Bennett DA, Blennow K, Carrillo MC, Dunn B, Haeberlein SB, Holtzman DM, Jagust W, Jessen F, Karlawish J, Liu E, Molinuevo JL, Montine T, Phelps C, Rankin KP, Rowe CC, Scheltens P, Siemers E, Snyder HM, Sperling R, Elliott C, Masliah E, Ryan L, Silverberg N (2018) NIA-AA Research Framework: Toward a biological definition of Alzheimer's disease. *Alzheimers Dement* **14**, 535-562.

[3] Gordon BA, Blazey TM, Su Y, Hari-Raj A, Dincer A, Flores S, Christensen J, McDade E, Wang G, Xiong C, Cairns NJ, Hassenstab J, Marcus DS, Fagan AM, Jack CR, Hornbeck RC, Paumier KL, Ances BM, Berman SB, Brickman AM, Cash DM, Chhatwal JP, Correia S, Förster S, Fox NC, Graff-Radford NR, la Fougère C, Levin J, Masters CL, Rossor MN, Salloway S, Saykin AJ, Schofield PR, Thompson PM, Weiner MM, Holtzman DM, Raichle ME, Morris JC, Bateman RJ, Benzinger TLS (2018) Spatial patterns of neuroimaging biomarker change in individuals from families with autosomal dominant Alzheimer's disease: A longitudinal study. *Lancet Neurol* **17**, 241-250.

[4] Horie K, Barthelemy NR, Mallipeddi N, Li Y, Franklin EE, Perrin RJ, Bateman RJ, Sato C (2020) Regional correlation of biochemical measures of amyloid and tau phosphorylation in the brain. *Acta Neuropathol Commun* **8**, 1-14.

[5] Mattson MP, Magnus T (2006) Ageing and neuronal vulnerability. *Nat Rev Neurosci* **7**, 278-294.

[6] Pfisterer U, Khodosevich K (2017) Neuronal survival in the brain: Neuron type-specific mechanisms. *Cell Death Dis* **8**, e2643.

[7] Matias I, Morgado J, Gomes FCA (2019) Astrocyte heterogeneity: Impact to brain aging and disease. *Front Aging Neurosci* **11**, 59.

[8] Saxena S, Caroni P (2011) Selective neuronal vulnerability in neurodegenerative diseases: From stressor thresholds to degeneration. *Neuron* **71**, 35-48.

[9] Cope TE, Rittman T, Borchert RJ, Jones PS, Vatansever D, Allinson K, Passamonti L, Vazquez Rodriguez P, Bevan-Jones WR, O'Brien JT, Rowe JB (2018) Tau burden and the functional connectome in Alzheimer's disease and progressive supranuclear palsy. *Brain* **141**, 550-567.

[10] Apostolova LG, Steiner CA, Akopyan GG, Dutton RA, Hayashi KM, Toga AW, Cummings JL, Thompson PM (2007) Three-dimensional gray matter atrophy mapping in mild cognitive impairment and mild Alzheimer disease. *Arch Neurol* **64**, 1489-1495.

[11] Apostolova LG, Thompson PM (2008) Mapping progressive brain structural changes in early Alzheimer's disease and mild cognitive impairment. *Neuropsychologia* **46**, 1597-1612.

[12] Whitwell JL, Przybelski SA, Weigand SD, Knopman DS, Boeve BF, Petersen RC, Jack CR, Jr. (2007) 3D maps from multiple MRI illustrate changing atrophy patterns as subjects progress from mild cognitive impairment to Alzheimer's disease. *Brain* **130**, 1777-1786.

[13] Dickerson BC, Sperling RA (2009) Large-scale functional brain network abnormalities in Alzheimer's disease: Insights from functional neuroimaging. *Behav Neurol* **21**, 63-75.

[14] Dipasquale O, Cercignani M (2016) Network functional connectivity and whole-brain functional connectomics to investigate cognitive decline in neurodegenerative conditions. *Funct Neurol* **31**, 191-203.

[15] Medaglia JD, Pasqualetti F, Hamilton RH, Thompson-Schill SL, Bassett DS (2017) Brain and cognitive reserve: Translation via network control theory. *Neurosci Biobehav Rev* **75**, 53-64.
[16] Smart CM, Spulber G, Garcia-Barrera M (2014) Structural brain changes evident in default mode network areas in older adults with subjective cognitive decline compared to healthy peers. *Alzheimers Dement* **10**, P608.
[17] Wu K, Taki Y, Sato K, Qi H, Kawashima R, Fukuda H (2013) A longitudinal study of structural brain network changes with normal aging. *Front Hum Neurosci* **7**, 113.
[18] Xiang J, Guo H, Cao R, Liang H, Chen J (2013) An abnormal resting-state functional brain network indicates progression towards Alzheimer's disease. *Neural Regen Res* **8**, 2789-2799.
[19] Yang D, Yan C, Nie F, Zhu X, Turja A, Zsembik L, Styner M, Wu G (2019) Joint identification of network hub nodes by multivariate graph inference. *MICCAI*, Shenzhen, China, pp. 590-598.
[20] Sepulcre J, Grothe MJ, Uquillas FdO, Ortiz-Terán L, Diez I, Yang H-S, Jacobs HI, Hanseeuw BJ, Li Q, El-Fakhri G (2018) Neurogenetic contributions to amyloid beta and tau spreading in the human cortex. *Nat Commun* **24**, 1910-1918.
[21] Zhang J, Yang D, He W, Wu G, Chen M (2020) A network-guided reaction-diffusion model of AT [N] biomarkers in Alzheimer's disease. *BIBE,* Cincinnati, OH, USA, pp. 222-229.
[22] Vogel JW, Iturria-Medina Y, Strandberg OT, Smith R, Levitis E, Evans AC, Hansson O, Alzheimer's Disease Neuroimaging Imaging, Swedish BioFinder Study (2020) Spread of pathological tau proteins through communicating neurons in human Alzheimer's disease. *Nat Commun* **11**, 1-15.
[23] Liu Q, Yang D, Zhang J, Wei Z, Wu G, Chen M (2021) Analyzing the spatiotemporal interaction and propagation of ATN biomarkers in Alzheimer's disease using longitudinal neuroimaging data. *ISBI,* Nice, France, pp. 126-129.
[24] Sporns O (2011) *Networks of the brain*, MIT Press.
[25] Fischl B (2012) FreeSurfer. *Neuroimage* **62**, 774-781.
[26] Destrieux C, Fischl B, Dale A, Halgren E (2010) Automatic parcellation of human cortical gyri and sulci using standard anatomical nomenclature. *Neuroimage* **53**, 1-15.
[27] Rubinov M, Sporns O (2010) Complex network measures of brain connectivity: Uses and interpretations. *Neuroimage* **52**, 1059-1069.
[28] Janeiro MH, Ardanaz CG, Sola-sevilla N, Dong J, Cortés-erice M (2021) Biomarkers in Alzheimer's disease. *Adv Lab Med* **2**, 27-37.
[29] Van Den Heuvel MP, Mandl RCW, Stam CJ, Kahn RS, Hulshoff Pol HE (2010) Aberrant frontal and temporal complex network structure in schizophrenia: A graph theoretical analysis. *J Neurosci* **30**, 15915-15926.
[30] Fornito A, Zalesky A, Bullmore ET (2016) *Fundamentals of brain network analysis*. Academic Press.
[31] Pereira JB, Ossenkoppele R, Palmqvist S, Strandberg TO, Smith R, Westman E, Hansson O (2019) Amyloid and tau accumulate across distinct spatial networks and are differentially associated with brain connectivity. *Elife* **8**, e50830.
[32] Sintini I, Graff-Radford J, Jones DT, Botha H, Martin PR, Machulda MM, Schwarz CG, Senjem ML, Gunter JL, Jack CR, Jr, Lowe VJ, Josephs KA, Whitwell JL (2020) Tau and amyloid relationships with resting-state functional connectivity in atypical Alzheimer's disease. *Cereb Cortex* **31**, 1693-1706.